Electronic Suppplementary Information

Identifying Electrocatalytic Active Sites of Ru-based Catalyst with High Faraday Efficiency in CO_2 saturated media for Aqueous Zn-CO_2 System

Jeongwon Kim,[1] Yejin Yang, [1] Arim Seong, [1] Hyuk-Jun Noh, [1] Changmin Kim, [1] Sangwook Joo, [1] Ara Cho, [2] Linjuan Zhang, [3] Jing Zhou, [3] Jian-Qiang Wang, [3] Jeong Woo Han, [2] Javeed Mahmood, [1,] Jong-Beom Baek, [1,*] and Guntae Kim[1,*]*

[1]School of Energy and Chemical Engineering,
Ulsan National Institute of Science and Technology (UNIST)
Ulsan, 44919, Republic of Korea

[2]Department of Chemical Engineering,
Pohang University of Science and Technology (POSTECH)
Pohang, Gyeongbuk 37673, Republic of Korea

[3]Key Laboratory of Interfacial Physics and Technology,
Shanghai Institute of Applied Physics, Chinese Academy of Sciences
Shanghai, 201800, People's Republic of China

[*] Correspndence: javeed@unist.ac.kr (J. M.), jbbaek@unist.ac.kr (J.-B. B.), gtkim@unist.ac.kr (G. K.)

Experimental Methods

Oxidation of porous sphere carbon (PSC). [1-4]

In a three-neck round bottom flask 10 g of carbon black (Alfa Aesar; S.A.: 75 m^2 g^{-1}, Bulk density: 170-230 g L^{-1}) was taken with concentrated nitric acid (500 mL) and sonicated for 1 hour to disperse the PSC in the nitric acid. The flask was transferred to oil bath and refluxed for 24 hours. After cooling down to ambient condition the mixture was poured into 1L of deionized water and the sample was collected by filtration. Then the sample was Soxhlet extraction with water and methanol to remove remnant acid and other impurities, if any. The sample was then freeze dried for 3 days at -120 °C under reduced pressure.

Preparation of CF-Ru@PSC.

To a 1.3 L of *N*-Methyl-2-Pyrrolidone (NMP) 10 g of oxidized PSC was added along with 3 g of ruthenium chloride ($RuCl_3$) and sonicated for 3 hours in bath sonicator. After sonication, the sample was stirred overnight on the magnetic stirrer and the dispersion was again sonicated for 2 hours to completely disperse PSC in NMP. Then 60 mL of sodium borohydride (10% solution in NMP) was added by dropping funnel under vigorous stirring condition, after the addition the solution was stirred again for 1 hour. Then the solution was mixed with 1.5 L acetone and filtered the precipitates and washed with water and freeze dried for 3 days at -120 °C under reduced pressure. After freeze drying the sample was annealed at different temperature (600, 700, 800, 900 °C) under Argon atmosphere for 2 hours. The samples were then washed with water after annealing to remove any unbound metal impurities in the matrix and dried again in the oven at 100 °C under the reduced pressure. The Non CF-Ru@PSC catalyst produced from same procedures with Ru@PSC excepting the oxidation process of PSC substrate.

Structural characterization and electrochemical measurements.

The crystal structures of Ru@PSC catalyst were conducted by using X-ray powder diffraction (XRD) (Rigaku diffractometer, Cu Kα radiation) and a scan rate of 1° min^{-1}. The

transmission electron microscopy (TEM) images were obtained using a high resolution-TEM (JEOL, JEM-2100F). XPS results were conducted on a Thermo Fisher K-alpha X-ray photoelectron spectrometer (UK). The surface area of sample was calculated by N_2 adsorption and desorption isotherms using the Brunauer-Emmett-Teller (BET) on BELSORP-max (BEL Japan, Inc., Japan). The weight content of Ru in Ru@PSC was analyzed from Thermogravimetric analysis (TGA) in air and at a ramping rate of 10 °C/min using a Thermogravimetric Analyzer Q200 TA Instrument, USA. Ru K-edge X-ray absorption spectroscopy (XAS) were conducted at beamline 14W1 of the Shanghai Synchrotron Radiation Facility (SSRF) and beamline 1W1B of the Beijing Synchrotron Radiation Facility (BSRF), China. Data were recorded using a Si (111) double crystal monochromator in transmission mode. All XAFS data were analyzed using the program Demeter.[5] For all samples, the EXAFS oscillations were extracted from the normalized XAS spectra by subtracting the atomic background using a cubic spline fit to k^2-weighted data, where k is the photoelectron wave number. The $\chi(k)$ functions were then Fourier transformed into R-space. The Fourier-transform window was in the k range 2–11 Å for Ru. The electrochemical measurements were conducted in three-electrode configuration using potentiostat (Biologic VMP3). The graphite rod was used as a counter electrode and Ag/AgCl (saturated KCl solution) electrode was used as a reference electrode. For detailed electrochemical analysis, RHE calibration was conducted with Pt wires and Ag/AgCl reference electrode (Fig. S23). The rotating disk electrode (RDE) was conducted as working electrode in RRDE-3A (ALS Co.). Each catalyst was prepared to ink solution by dispersing 10 mg of the catalyst in 1 mL solution (ethanol: isopropyl alcohol = 1:1) with 5 mg Nafion. The glassy carbon disk electrode in RDE was coated by drop-coating of 5μL of the catalyst ink. All half-cell profiles were *i*R compensated by measuring the resistance of the solution. Accelerated stability measurements were conducted with continuous potential cycling from – 0.35 V to 0.15 V vs. RHE at a scan rate of 100 mV s^{-1}.

The underpotential deposition (UPD) of copper on Pt and Ru was conducted to calculate the active sites of each catalyst. The number of active sites (n) was qualified based on the UPD copper stripping charge (Q_{cu}, $Cu_{upd} \rightarrow Cu^{2+} + 2e^-$) as follow:

$$n = Q_{cu}/2F$$

where F is the Faraday constant (C mol^{-1})

The turnover frequency (TOF, s^{-1}) was calculated with the following equation:

$$TOF = I/(2Fn)$$

Where I is the current (A) from LSV measurements for HER, F is the Faraday constant (C mol^{-1}), n is the number of active sites (mol) from UPD measurements. The ½ value is attributed from two electrons required to evolve one hydrogen molecule.

The aqueous Zinc-CO_2 system is fabricated with H-type cell. The system is fabricated of Zinc metal / alkaline electrolyte / membrane / aqueous electrolyte / cathode. For alkaline electrolyte, the 6 M KOH was used and Nafion 212 membrane was used as separator between alkaline and aqueous electrolyte. The aqueous electrolyte was composed with CO_2-saturated 1 M KOH solution. The cathode was prepared by drop-coating on the carbon paper, TGP-H-090 (Toray carbon paper). The loading density of each catalyst was 2 mg cm^{-2} using ink solution. All electrochemical measurements were investigated using Biologic VMP 3. The generated gas (H_2) was analyzed by gas chromatograph (Agilent 2820A GC instrument) with a thermal conductivity detector (TCD) and a packed column (Agilent carboxen 1000). The gas was quantitively controlled using a mass flow controller (Atovac GMC1200).

Computational Details

Density functional theory (DFT) calculations were performed with the Vienna ab initio simulation package (VASP). [6-8] The Perdew−Burke−Ernzerhof (PBE) parametrization of the generalized gradient approximation (GGA) was used as exchange-correlation functional.[9] A plane-wave basis set with a cut off energy of 400 eV was used. The Brillouin zone was sampled using a 1 × 1 × 1 *k*-point grid for Ru@PSC and 6 × 6 × 1 *k*-point grid for both

Pt(111) and Ru(0001) in the Monkhorst−Pack scheme. The Ru@PSC structure consists of Ru_{13} particle on a (7 × 7) graphene supercell sheet with a vacuum of 30 Å in the z-direction because Ru_{13} particle represented well the hydrogen adsorption energy of Ru slab.[4] For Ru(0001) and Pt(111), (2 × 2) surface unit cells with five layers were employed with a vacuum of 15 Å in the z-direction while bottom two layers were fixed. The atomic charge distribution of Ru@PSC was estimated by employing the Bader charge analysis.[10] The Gibbs free energy change was calculated as $\Delta G = \Delta E + \Delta ZPE - T\Delta S$, where ΔE is the reaction energy obtained from the DFT calculations, ΔZPE is the DFT-calculated zero-point energy, *S* is the standard entropy taken from NIST Chemistry WebBook, and T is set to 298.15 K.[11]

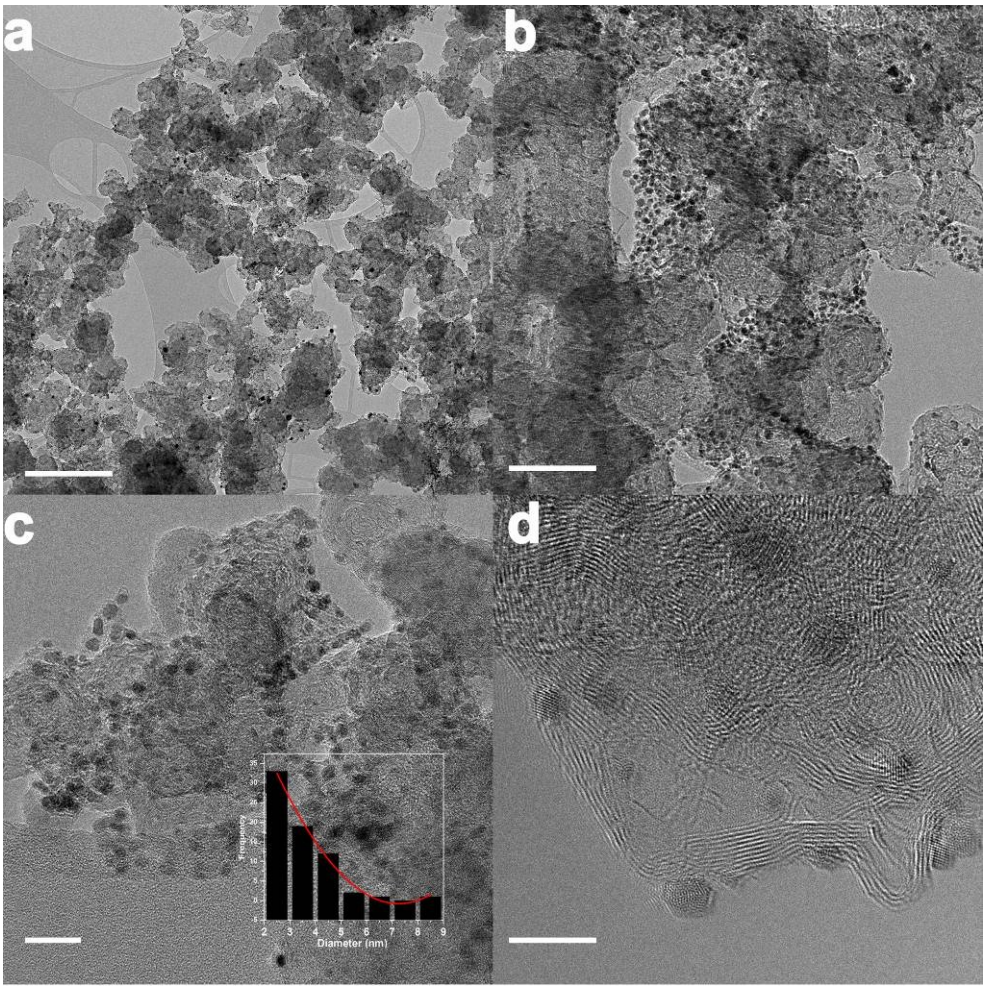

Fig. S1. a, b) Low-resolution TEM image and c, d) high-resolution TEM image of CF-Ru@PSC annealed at 600 ^{O}C. Inset in S1c: corresponding Ru particle distribution. Scale bar: a) 200 nm, b) 50 nm, c) 20 nm, and d) 10 nm

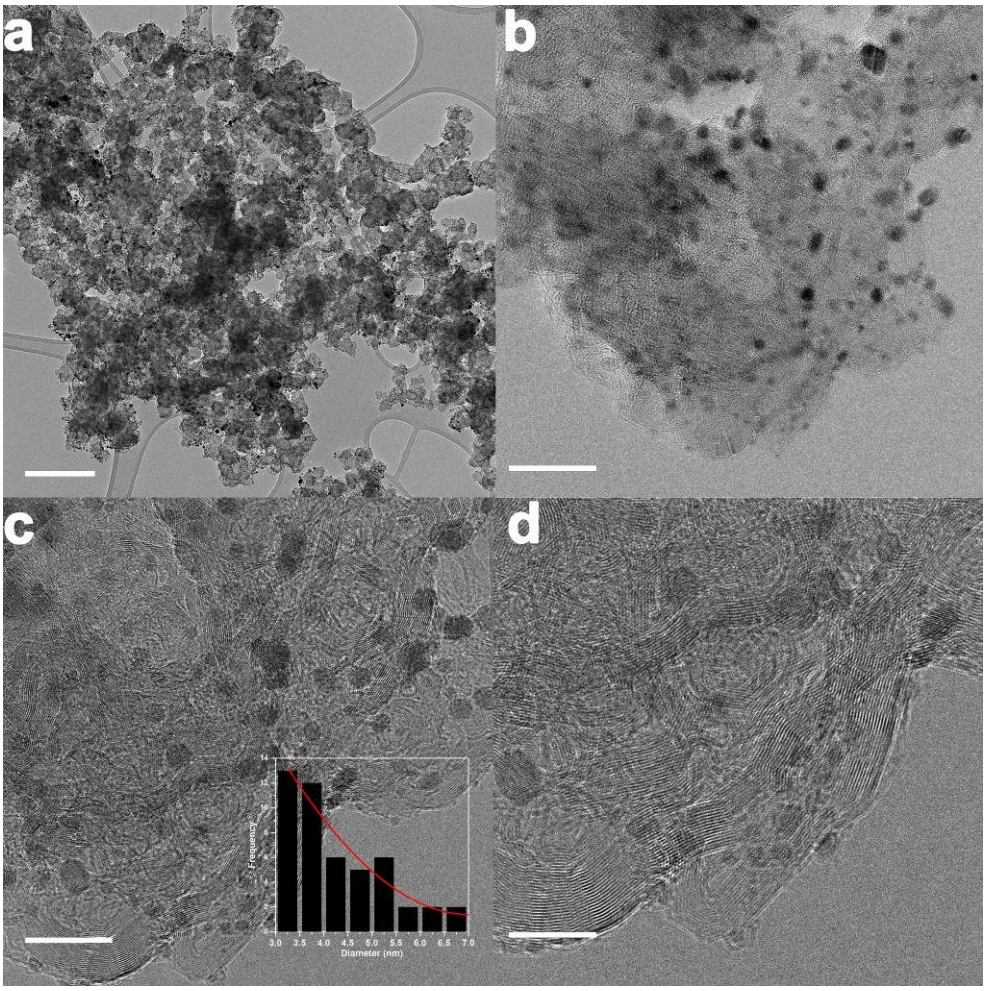

Fig. S2. a) Low-resolution TEM image and b-d) high-resolution TEM image of CF-Ru@PSC annealed at 800 ^{O}C. Inset in S2c: corresponding Ru particle distribution. Scale bar: a) 200 nm, b) 20 nm, c) 20 nm, and d) 10 nm

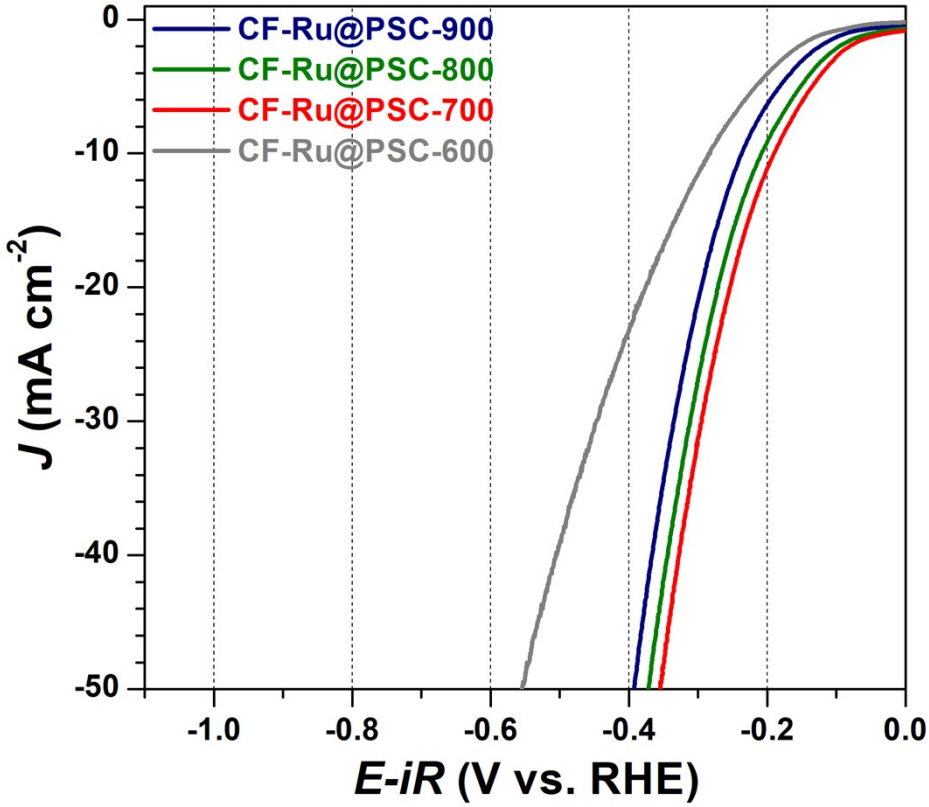

Fig. S3. Polarization curves of CF-Ru@PSC catalysts in CO_2-saturated 1 M KOH with respect to annealing temperature from 600 to 900 °C.

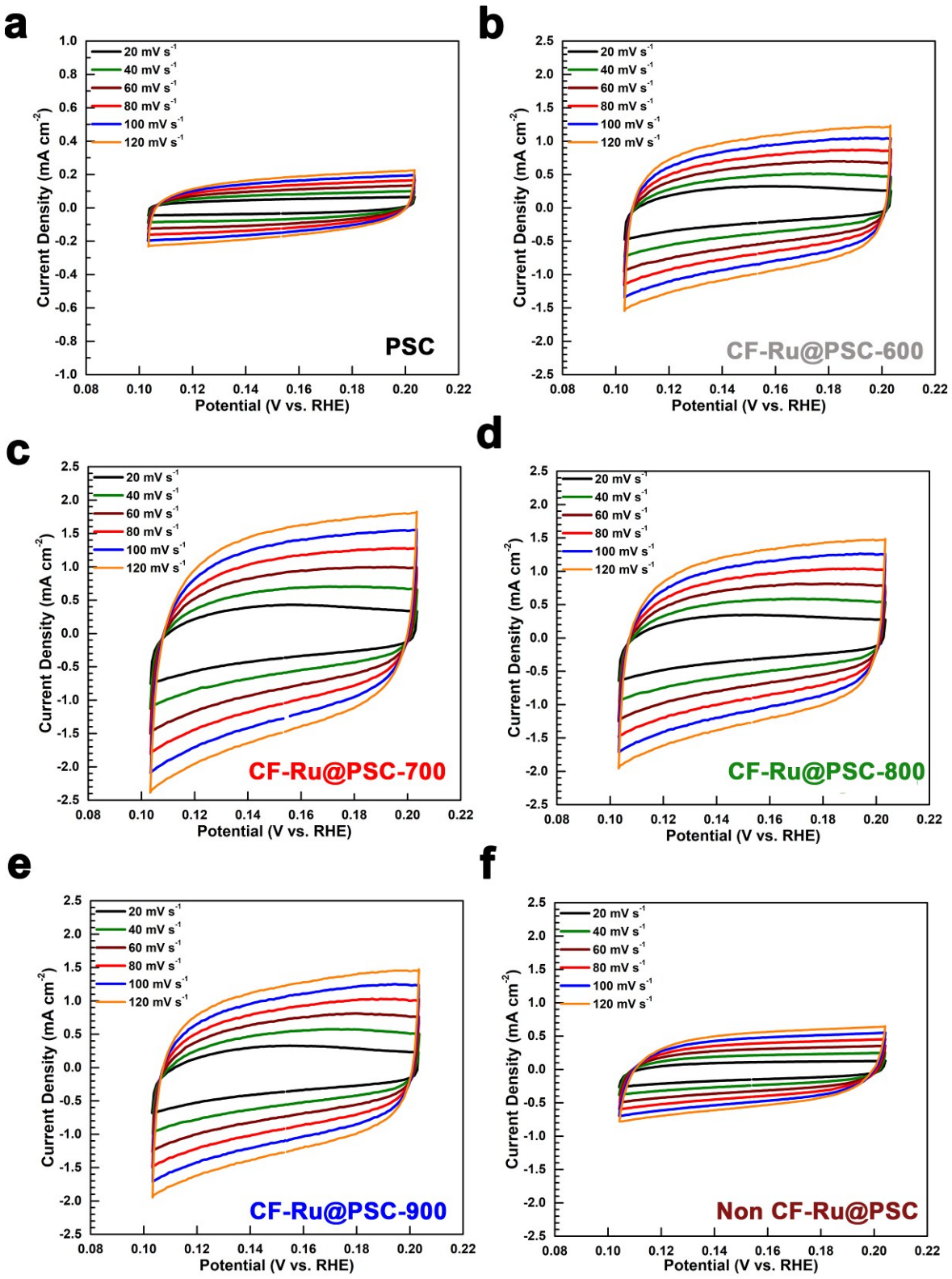

Fig. S4. Electrochemical CV scans recorded for **a**) PSC substrate, **b**) CF-Ru@PSC 600, **c**) CF-Ru@PSC 700, **d**) CF-Ru@PSC 800, **e**) CF-Ru@PSC 900, and **f**) NC CF-Ru@PSC. The selected potential range where no faradic current was observed is 0.1 to 0.2 V vs. RHE.

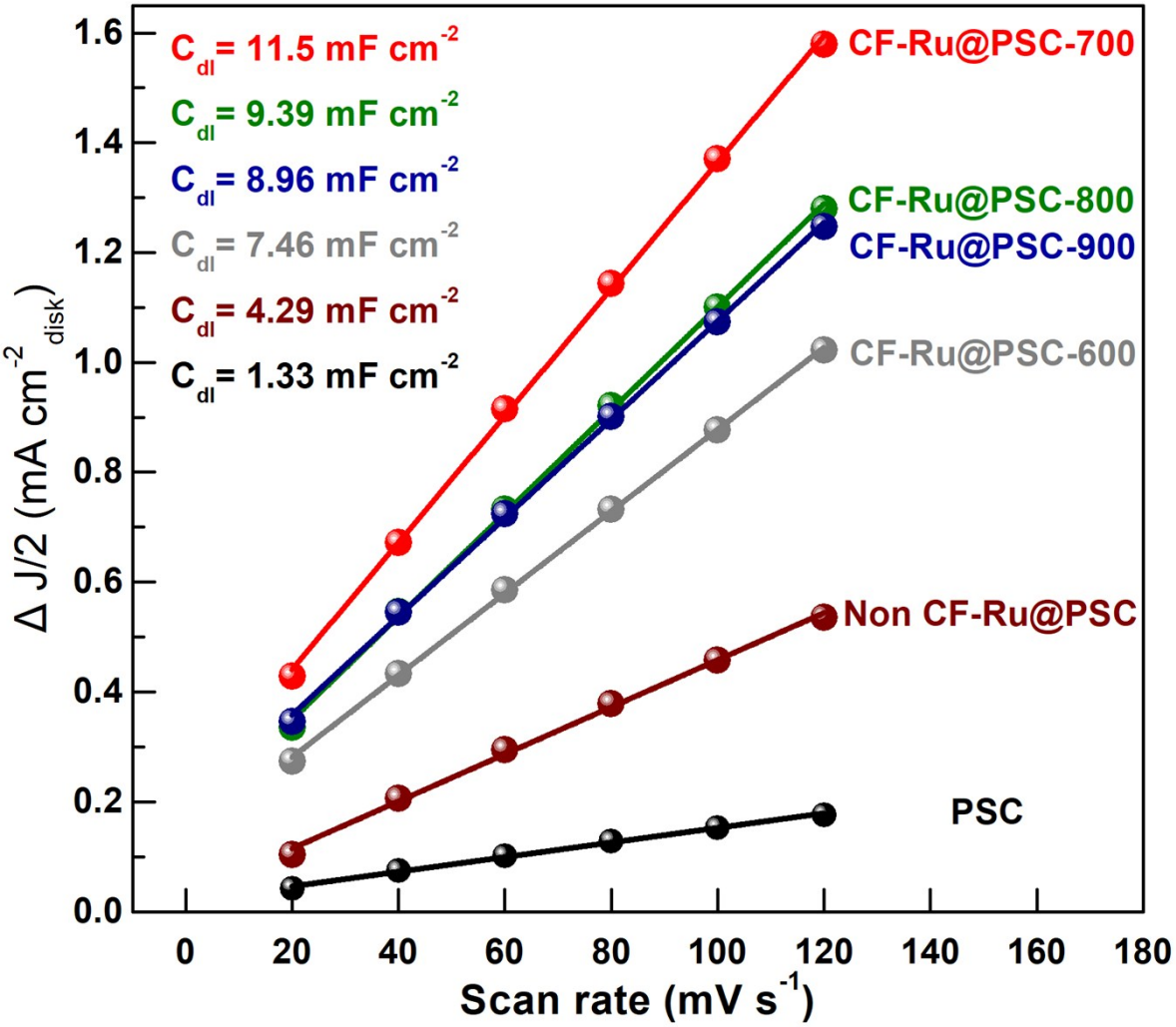

Fig. S5. Plot of half of the non-faradaic current density at 0.15 V vs. the scan rate of each catalyst in Fig. SS4.

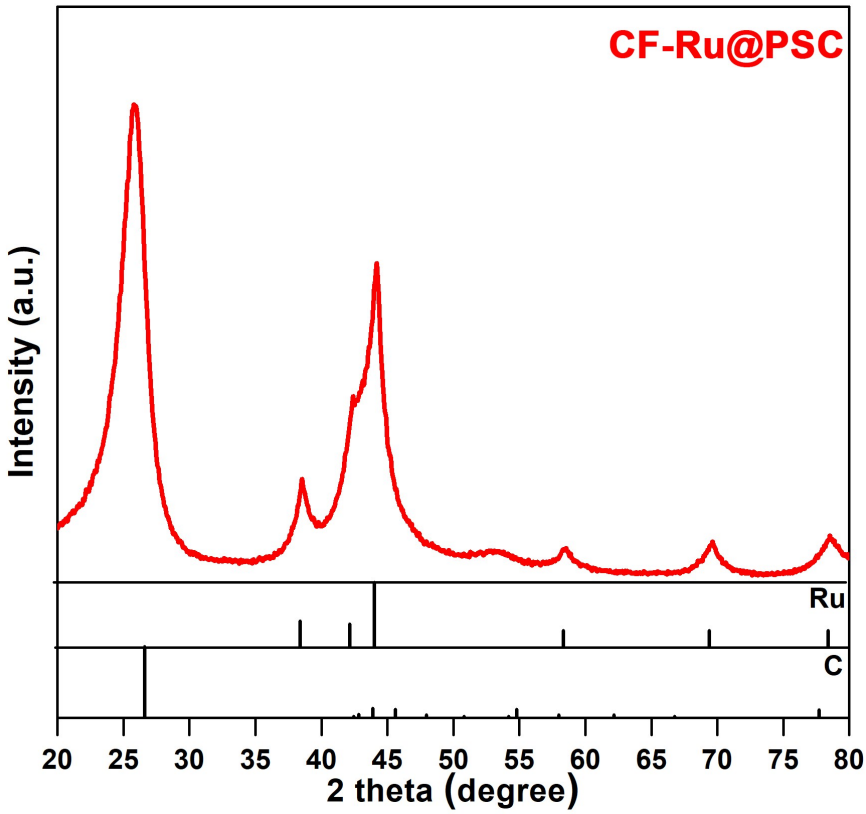

Fig. S6. Powder XRD pattern of CF-Ru@PSC.

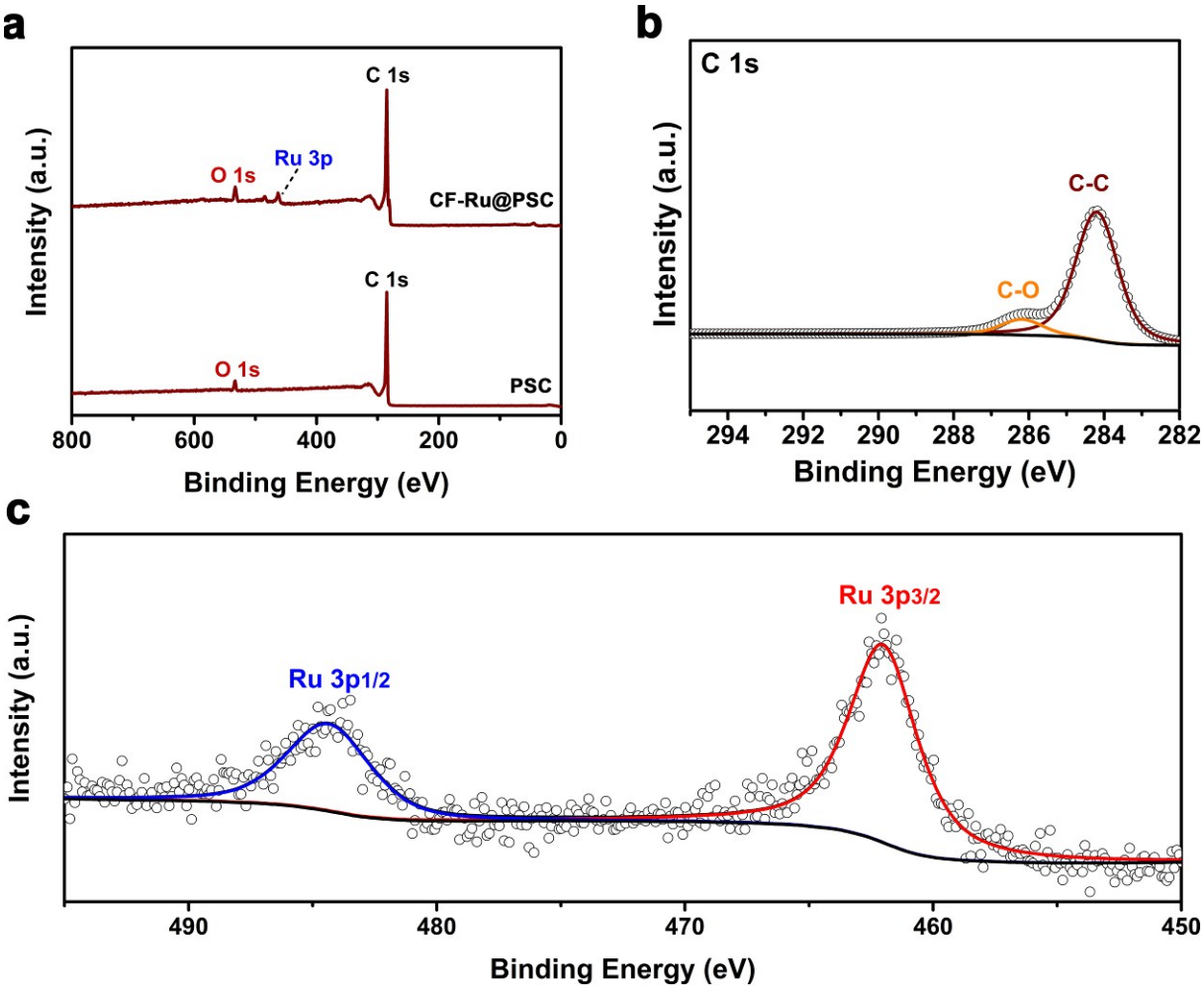

Fig. S7. **a**) XPS survey spectrum of CF-Ru@PSC and PSC. High-resolution XPS spectra of the **b**) C 1s, and **c**) Ru 3p in CF-Ru@PSC catalyst.

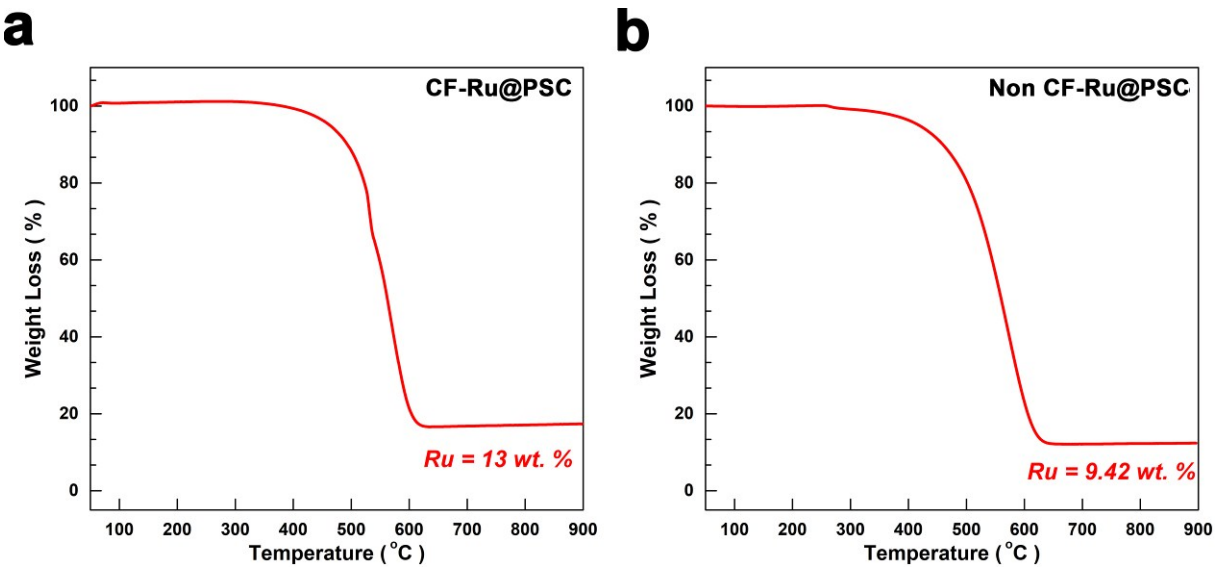

Fig. S8. TGA profile of a) CF-Ru@PSC and b) Non CF-Ru@PSC catalyst under air condition with a ramping rate of 10 °C min^{-1}.

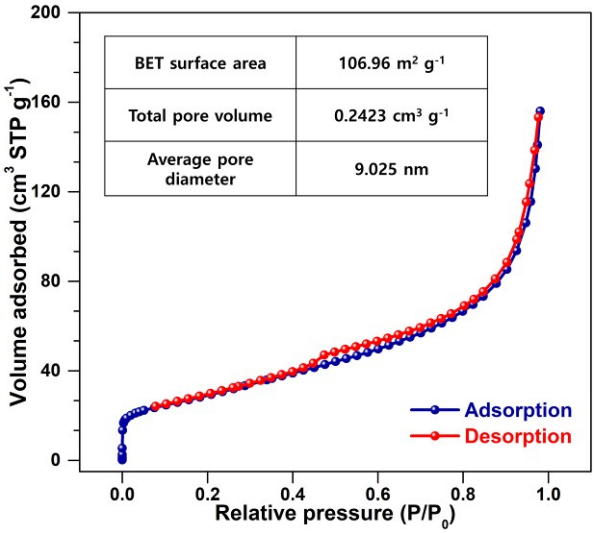

Fig. S9. N_2 adsorption/desorption isotherm of the CF-Ru@PSC catalyst.

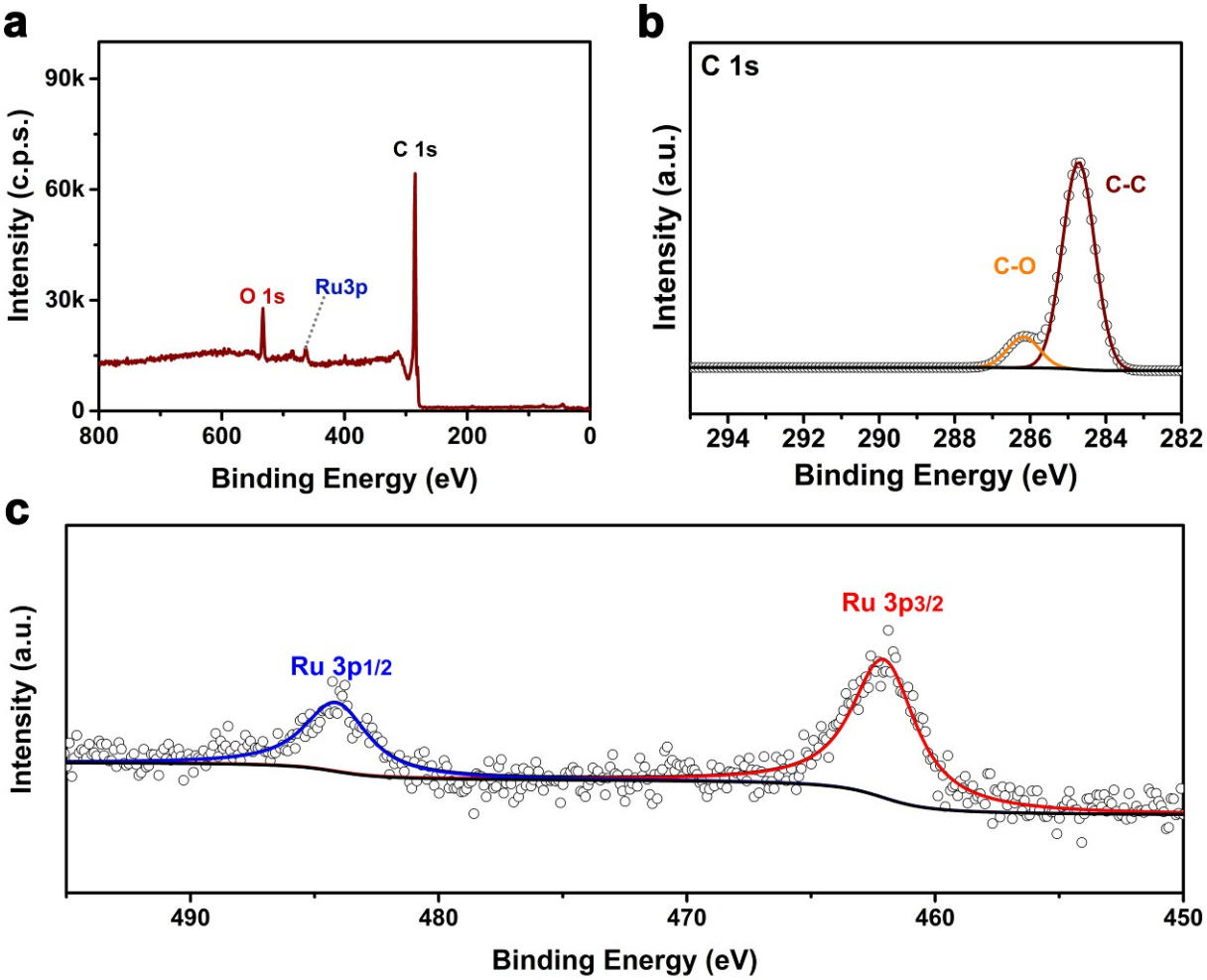

Fig. S10. **a**) XPS survey spectrum, high-resolution XPS spectra of the **b**) C 1s, and **c**) Ru 3p in Non CF-Ru@PSC catalyst.

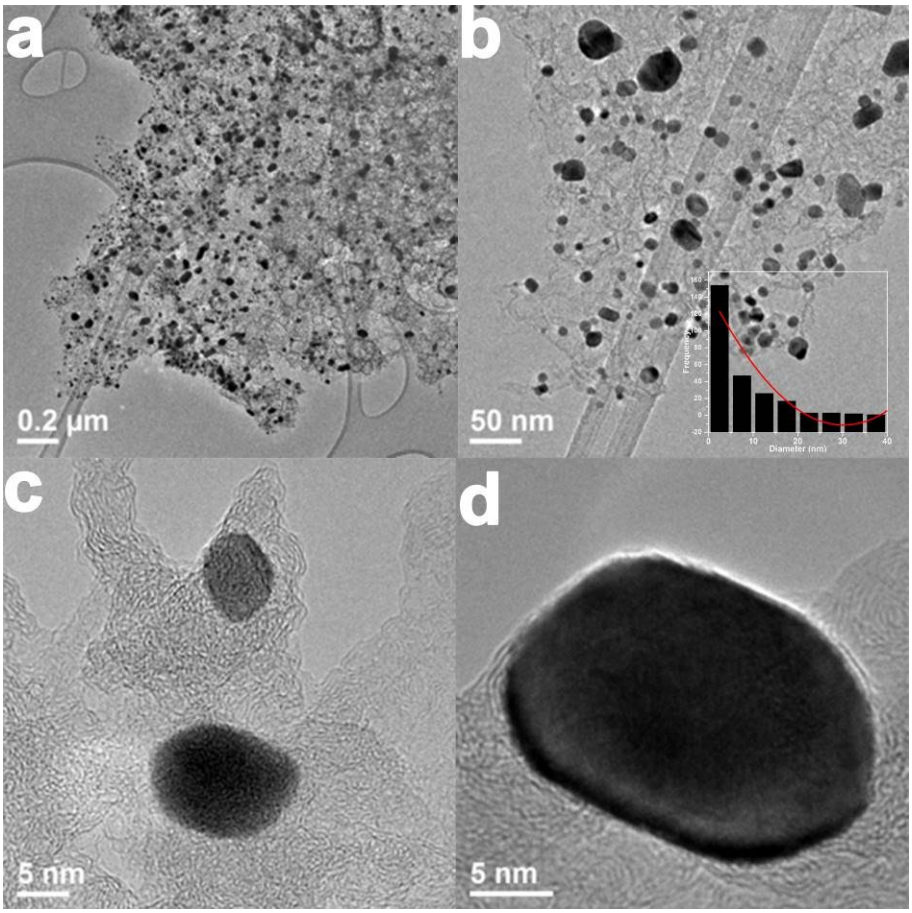

Fig. S11. a, b) Low-resolution TEM image and c, d) high-resolution TEM image of Non CF-Ru@PSC annealed at 700 ^{O}C. Inset in S9b: corresponding Ru particle distribution.

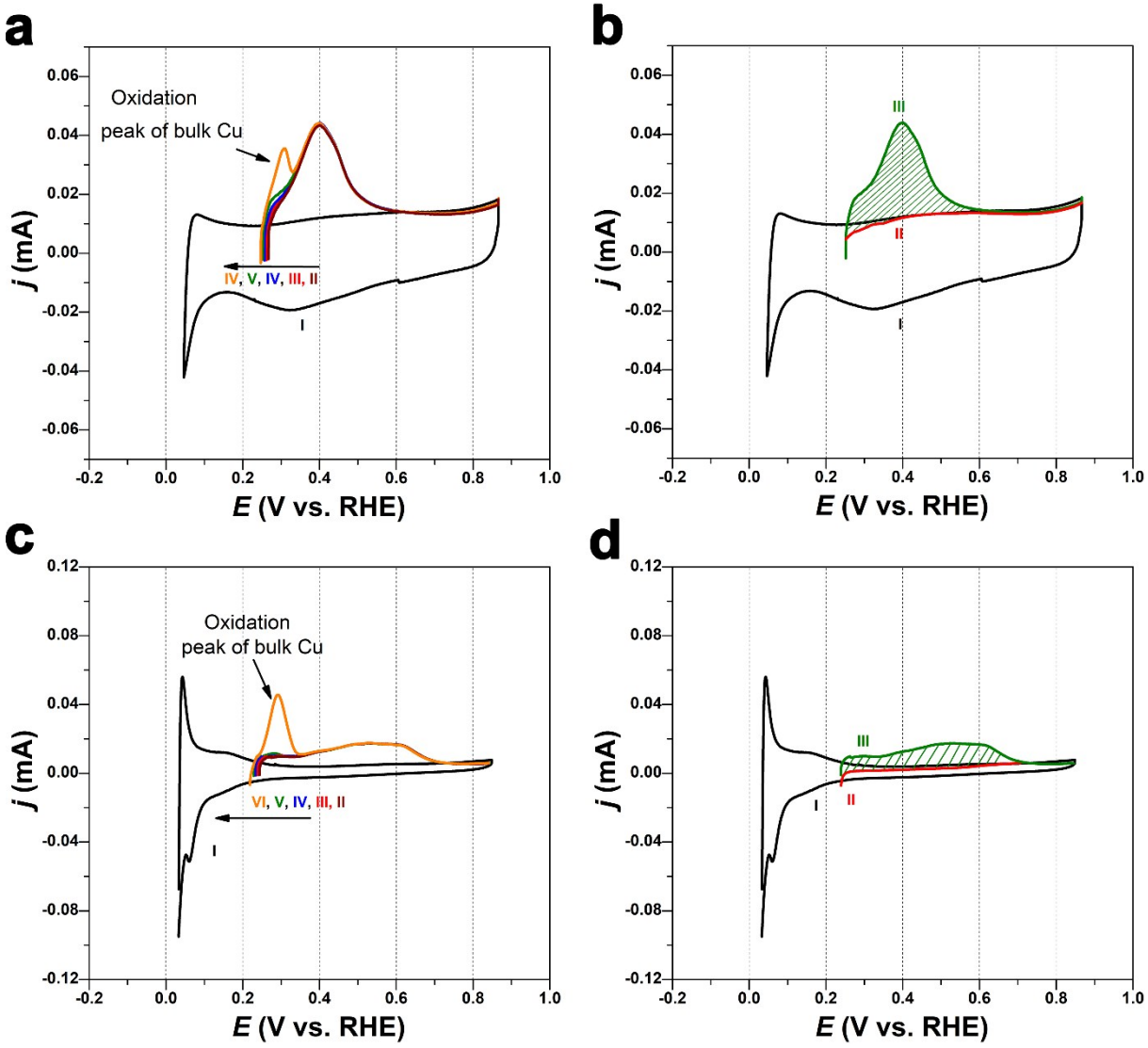

Fig. S12. **a**) Copper UPD in 0.5 M H_2SO_4 in the (I) absence and (II-VI) presence of 5 mM $CuSO_4$ on CF-Ru@PSC catalyst. For II-VI, the electrode was polarized at 0.250, 0.245, 0.240, 0.235, and 0.230 V for 100 s to form the UPD layers, respectively. **b**) Copper UPD in 0.5 M H_2SO_4 in the (I, II) absence and (III) presence of 5 mM $CuSO_4$ on CF-Ru@PSC catalyst. For II and III, the electrode was polarized at 0.240 V for 100 s to form the UPD layer. **c**) Copper UPD in 0.5 M H_2SO_4 in the (I) absence and (II-VI) presence of 5 mM $CuSO_4$ on Pt/C. For II-VI, the electrode was polarized at 0.245, 0.240, 0.235, 0.230, and 0.220 V for 100 s to form the UPD layers, respectively. **d**) Copper UPD in 0.5 M H_2SO_4 in the (I, II) absence and (III) presence of 5 mM $CuSO_4$ on CF-Ru@PSC catalyst. For II and III, the electrode was polarized at 0.240 V for 100 s to form the UPD layer.

As shown in Fig. S12a, there is only one oxidation peak around 0.4 V, indicating the oxidation reaction of deposited mono- or submonolayer copper. For a detailed calculation of the number of active sites, the bulk peak of Cu should be disappeared. To obtain a monolayer copper, 0.240 V was selected in the following test of CF-Ru@PSC in Fig. SS12b. Pt/C catalyst was also investigated using the same method (Fig. S12c-d).

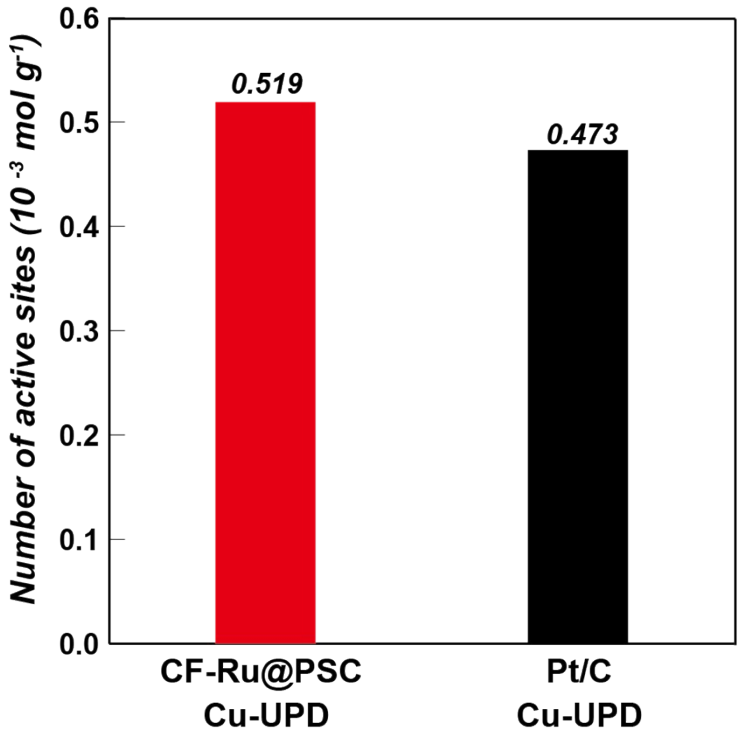

Fig. S13. The number of active sites in CF-Ru@PSC and Pt/C are calculated from Cu-UPD measurements in Fig. S12.

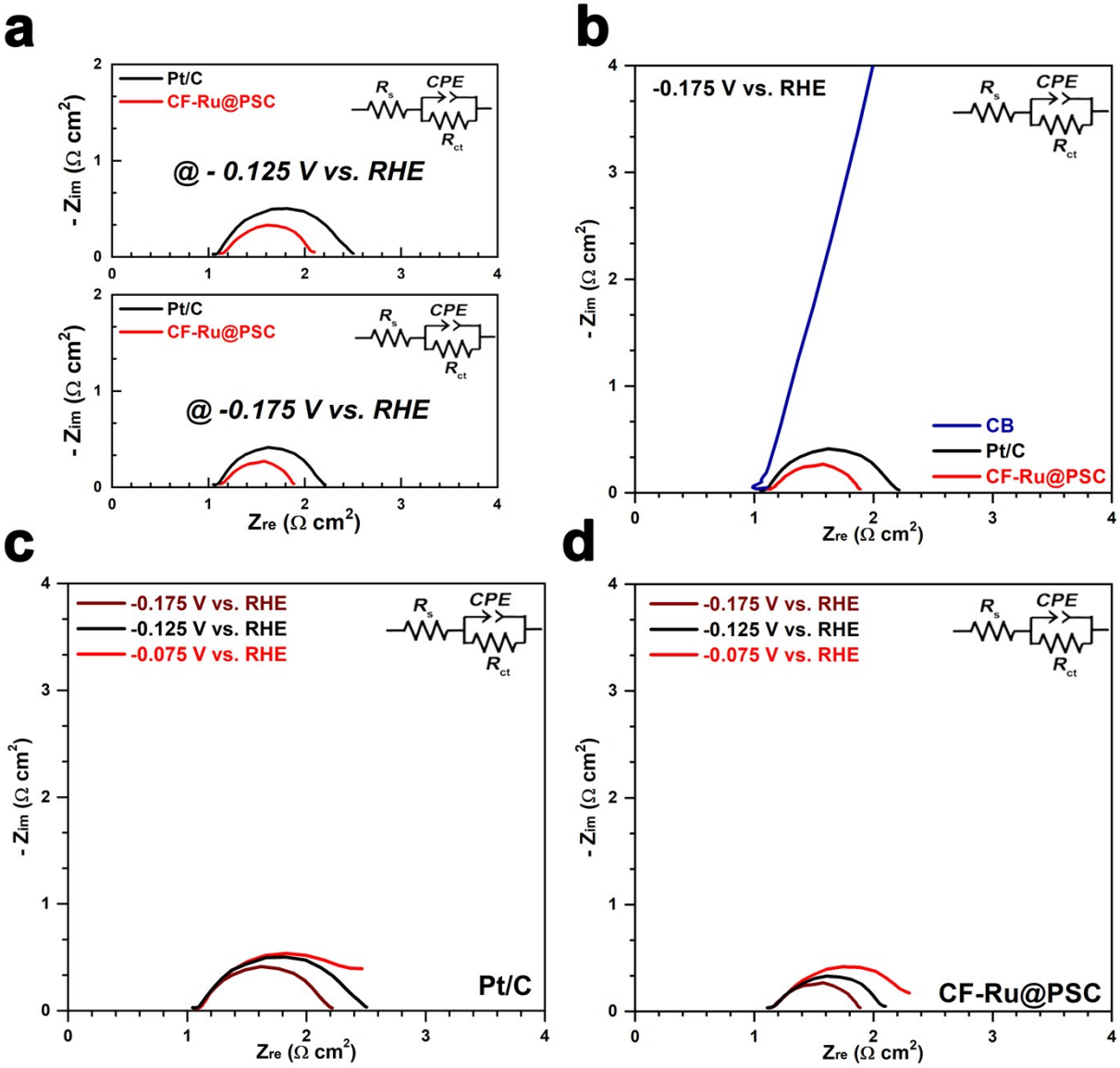

Fig. S14. EIS curves at -0.175 and -0.125 V *vs.* RHE of **a**) commercial Pt/C and CF-Ru@PSC catalyst. **b**) EIS curves at -0.175 of Pt/C, PSC, and CF-Ru@PSC. EIS curves at -0.175 V, -0.125 V, and -0.075 V vs. RHE of Pt/C and CF-Ru@PSC catalyst.

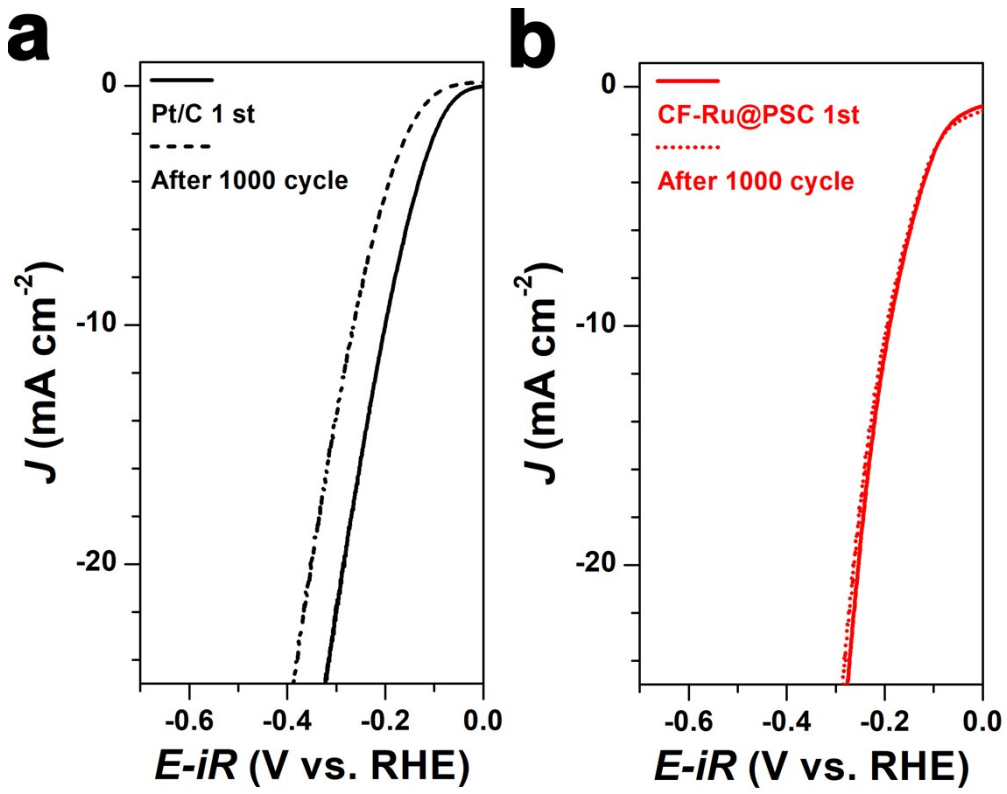

Fig. S15. Short-term durability test of a) Pt/C and b) CF-Ru@PSC catalyst. The polarization curves were conducted before and after 1,000 potential cycles in CO_2 saturated 1 M KOH solution from -0.35 V to 0.15 V *vs.* RHE.

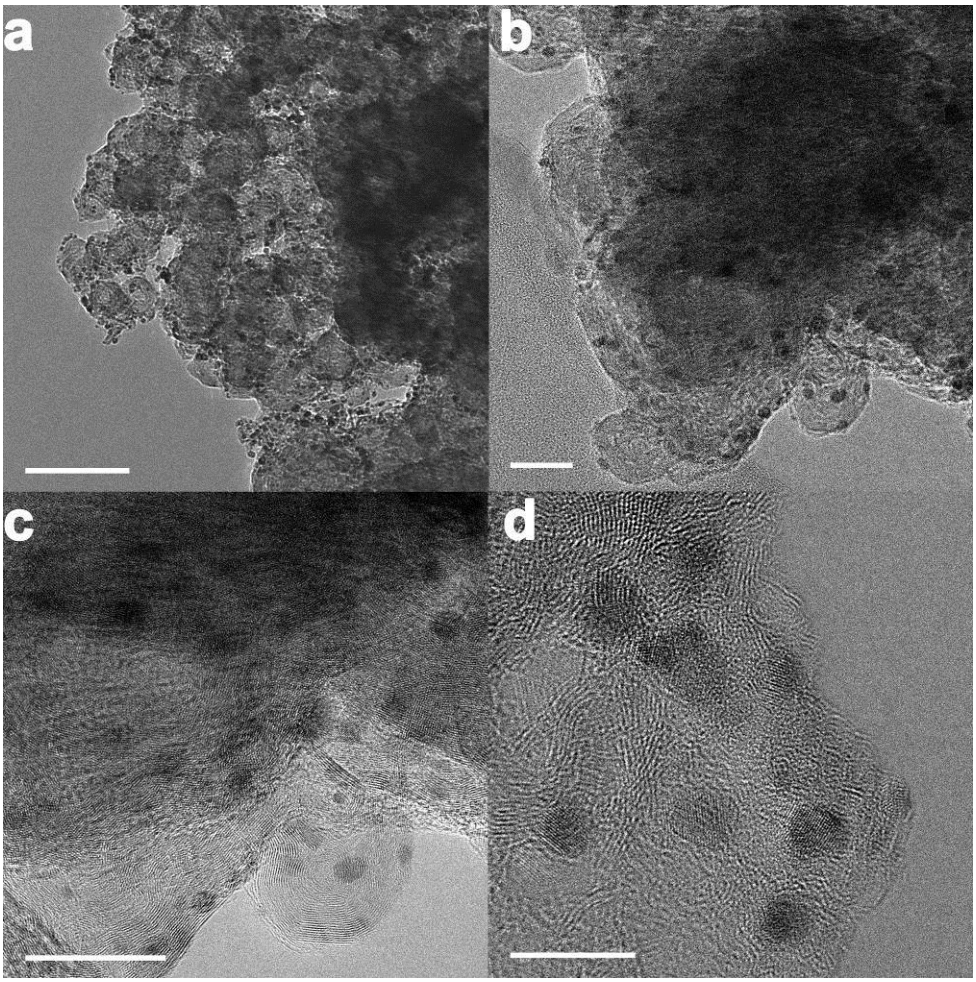

Fig. S16. a) Low-resolution TEM image and b-d) high-resolution TEM image of CF-Ru@PSC catalyst after long-term durability test. Scale bar: a) 100 nm, b) 20 nm, c) 20 nm, and d) 10 nm

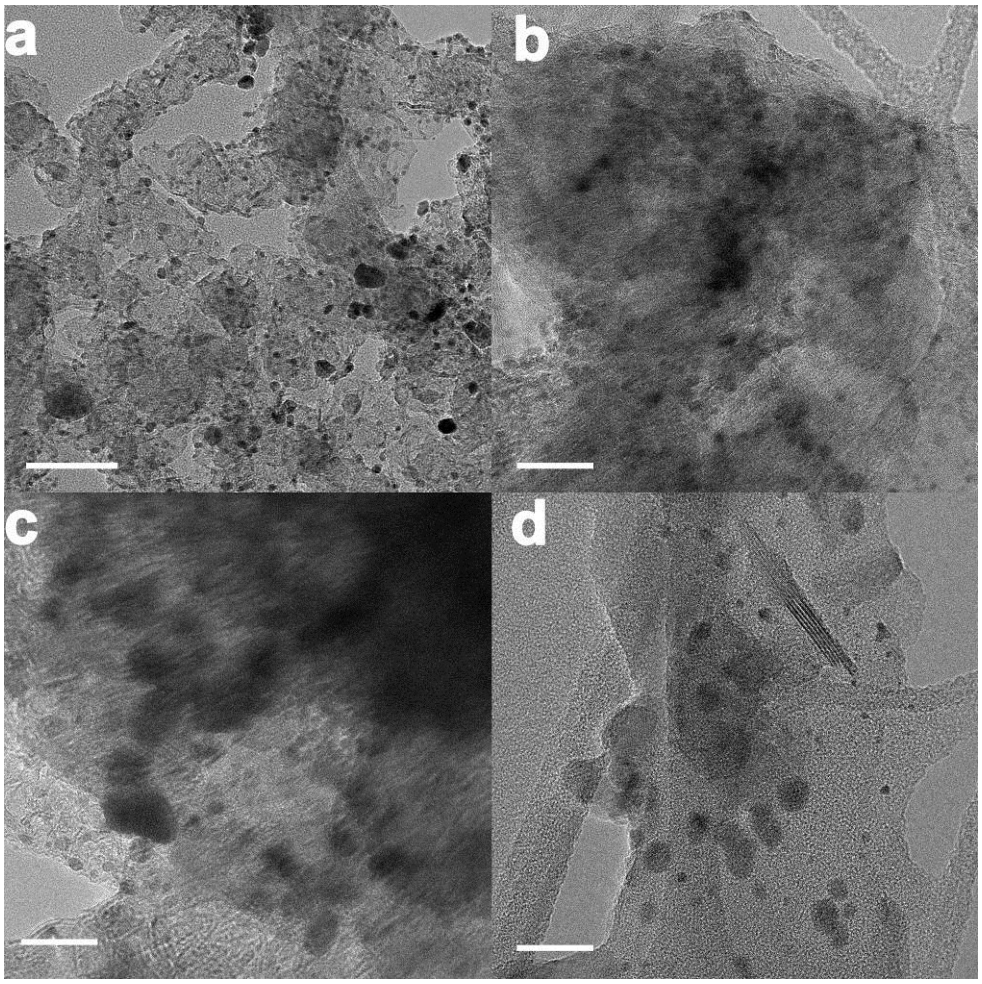

Fig. S17. a) Low-resolution TEM image and b-d) high-resolution TEM image of Pt/C catalyst after long-term durability test. Scale bar: a) 50 nm, b) 20 nm, c) 20 nm, and d) 20 nm

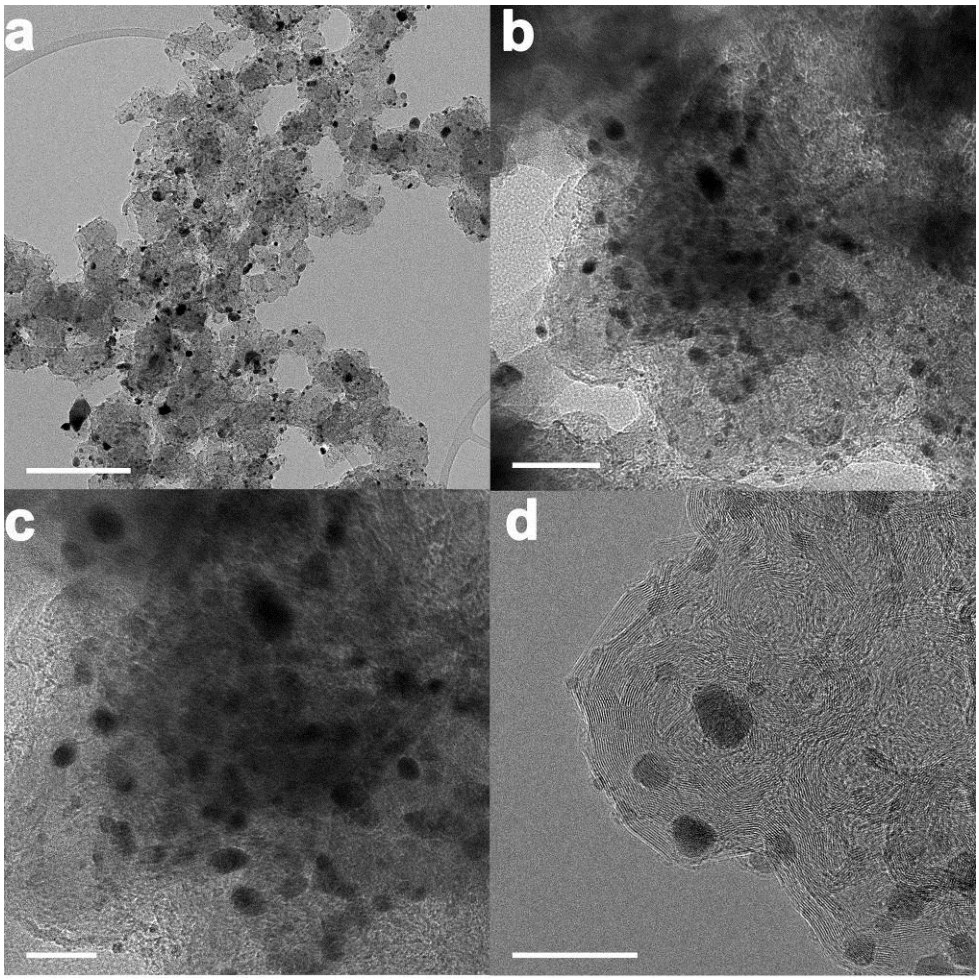

Fig. S18. a,b) Low-resolution TEM image and c,d) high-resolution TEM image of Non CF-Ru@PSC catalyst after long-term durability test. Scale bar: a) 200 nm, b) 50 nm, c) 20 nm, and d) 20 nm

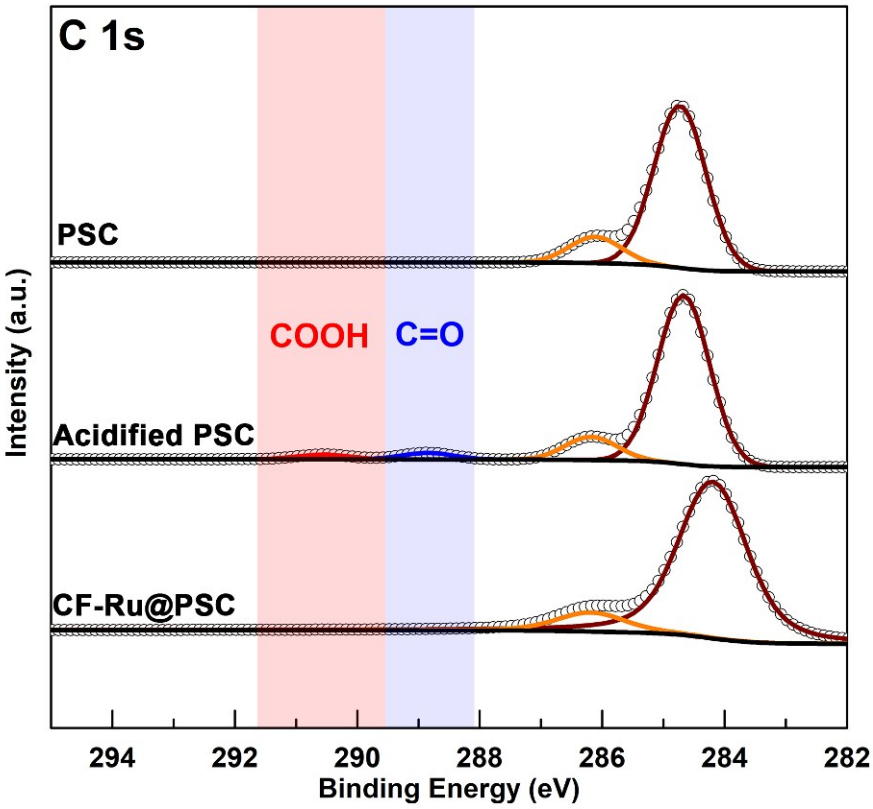

Fig. S19. High-resolution XPS spectra of the C 1s in PSC, Acidified PSC and CF-Ru@PSC catalyst.

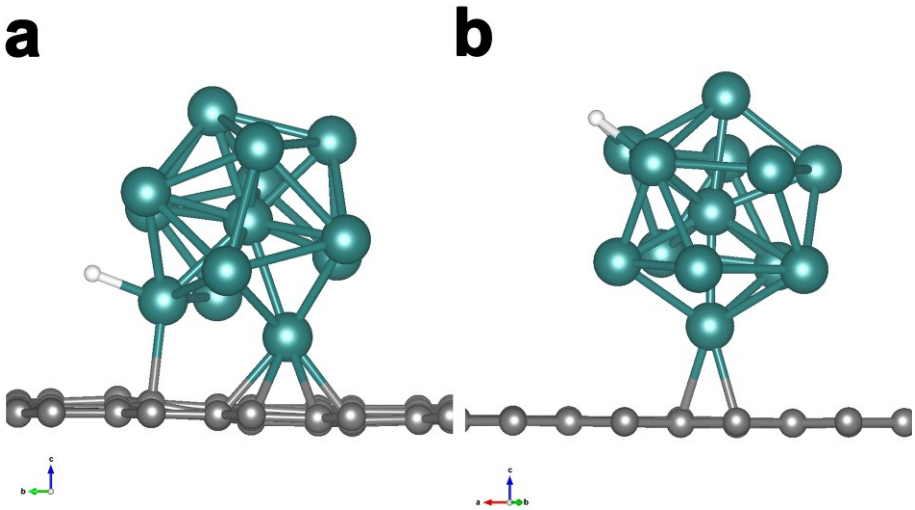

Fig. S20. Hydrogen adsorption configuration a) near and b) far from the graphene sheet.

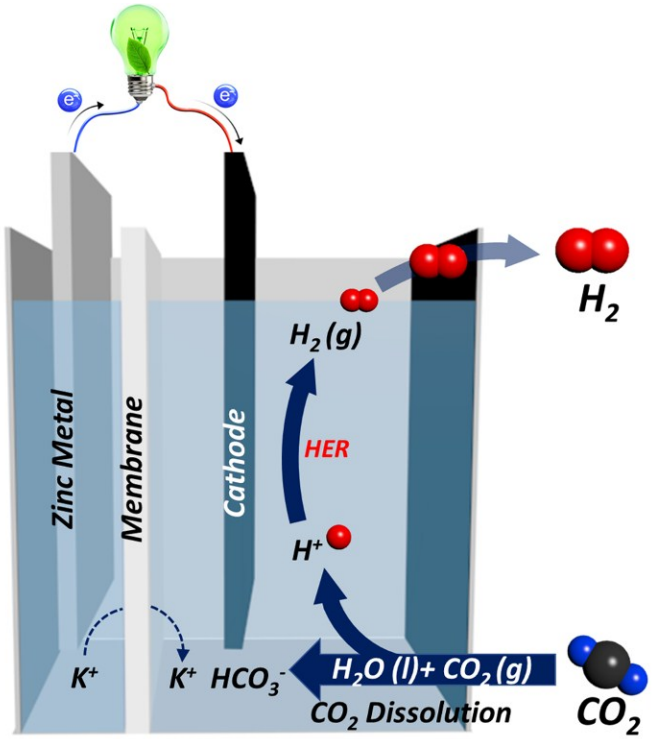

Fig. S21. Schematic illustration of aqueous Zn-CO_2 system.

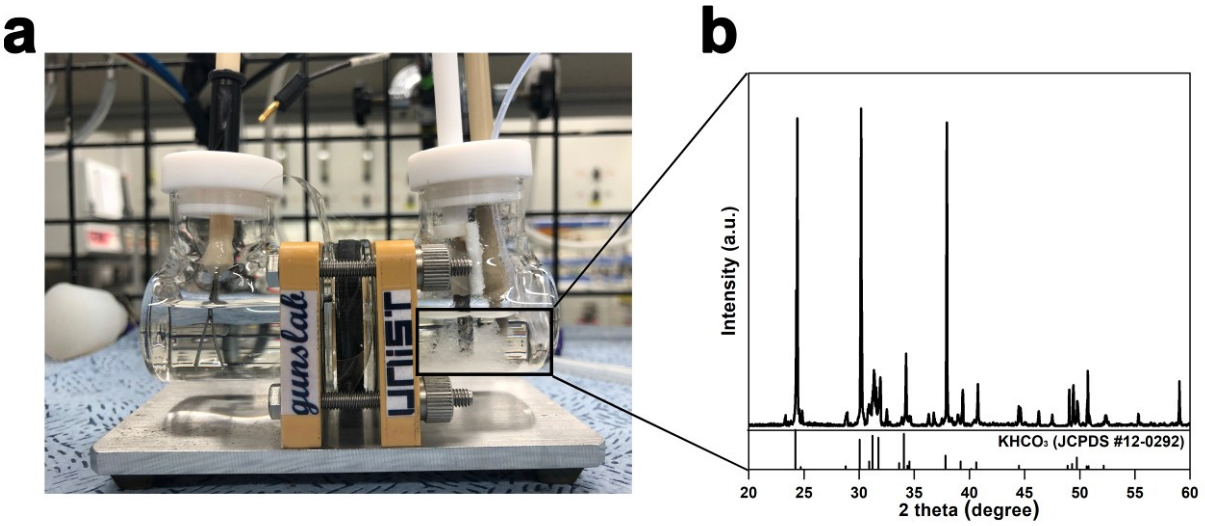

Fig. S22. (a) The digital photograph of aqueous Zn-CO_2 system after long-term stability test with CF-Ru@PSC catalyst. (b) The XRD profile of the precipitated white solid

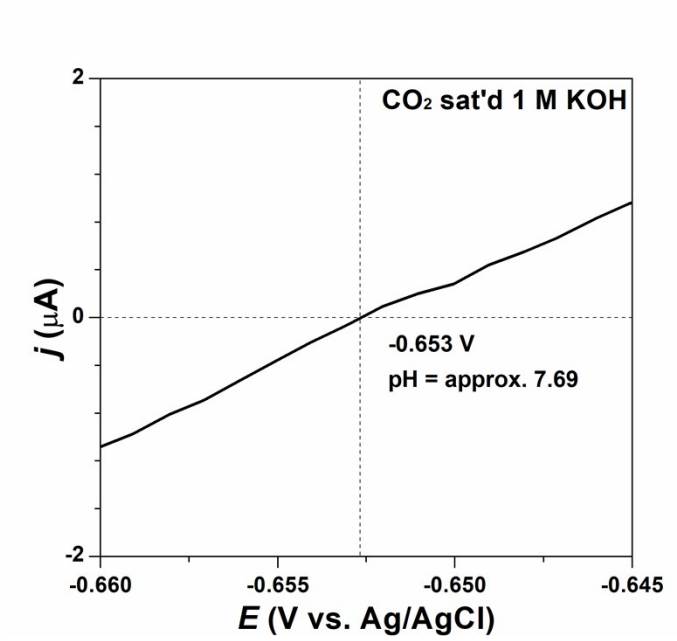

Fig. S23. RHE calibration. The potential was swept at 1 mV s^{-1} in H_2-saturated 0.1 M KOH. The open circuit potential was measured at -0.653 V vs Ag/AgCl. Pt wires were used as working and counter electrodes while Ag/AgCl was used as a reference electrode.

Table S1. Price of different noble metals

Metal	Symbol	Unit of Measure	U.S.
Platinum	Pt	troy ounce	$ 943.00
Palladium	Pd	troy ounce	$ 1652.00
Rhodium	Rh	troy ounce	$ 5400.00
Iridium	Ir	troy ounce	$ 1485.00
Ruthenium	Ru	troy ounce	$ 255.00
Osmium	Os	troy ounce	$ 400.00
Gold	Au	troy ounce	$ 1501.00

* The prices for various noble metals are from the BASF corporation website on 22/10/2019 (https://apps.catalysts.basf.com/apps/eibprices/mp/)

References

1 Ternero-Hidalgo, J. J., Rosas, J. M., Palomo, J., Valero-Romero, M. J., Rodríguez-Mirasol, J., and Cordero, T. (2016). Functionalization of activated carbons by HNO3 treatment: Influence of phosphorus surface groups. Carbon *101*, 409-419.

2 Kamegawa, K., Nishikubo, K., Kodama, M., Adachi, Y., and Yoshida, H. (2002). Oxidative degradation of carbon blacks with nitric acid: II. Formation of water-soluble polynuclear aromatic compounds. Carbon *40*, 1447-1455.

3 Papirer, E., Dentzer, J., Li, S., and Donnet, J. B. (1991). Surface groups on nitric acid oxidized carbon black samples determined by chemical and thermodesorption analyses. Carbon 29, 69-72.

4 Kamegawa, K., Nishikubo, K., and Yoshida, H. (1998). Oxidative degradation of carbon blacks with nitric acid (I)—Changes in pore and crystallographic structures. Carbon 36, 433-441.

5 Ravel, B., and Newville, M. J. (2005). ATHENA, ARTEMIS, HEPHAESTUS: data analysis for X-ray absorption spectroscopy using IFEFFIT. Synchrotron Rad. 12, 537-541.

6 Kresse, G., and Furthmuller, J. (1996). Efficient iterative schemes for ab initio total-energy calculations using a plane-wave basis set. Physical Review B *54*, 11169-11186.

7 Kresse, G., and Hafner, J. (1993). Ab initio molecular dynamics for liquid metals. Physical Review B *47*, 558-561.

8 Kresse, G., and Hafner, (1994). Norm-conserving and ultrasoft pseudopotentials for first-row and transition elements. J. Journal of Physics: Condensed Matter 6, 8245-8257.

9 Perdew, J. P., Burke, K., and Ernzerhof, M. (1996). Generalized Gradient Approximation Made Simple. Phys. Rev. Lett. 77, 3865-3868.

10 Sanville, E., Kenny, S. D., Smith, R., and Henkelman, G. (2007). Improved grid-based algorithm for Bader charge allocation. Journal of Computational Chemistry 28, 899-908.

11 N. I. O. Standards, Technology, NIST Chemistry Webbook: NIST Standard Reference Database Number 69. NIST: 2000.